MOX–Report No. 57/2014

Branching instability in expanding bacterial colonies

Giverso, C.; Verani, M.; Ciarletta P.;

MOX, Dipartimento di Matematica "F. Brioschi"
Politecnico di Milano, Via Bonardi 9 - 20133 Milano (Italy)

mox@mate.polimi.it http://mox.polimi.it

Branching instability in expanding bacterial colonies.

Chiara Giverso[1,2], Marco Verani[1] and Pasquale Ciarletta[2,3]

November 16, 2014

[1] MOX– Modellistica e Calcolo Scientifico
Dipartimento di Matematica "F. Brioschi"
Politecnico di Milano, Milano, Italy
chiara.giverso@polimi.it

[2] Fondazione Centro Europeo Nanomedicina
Piazza Leonardo da Vinci, 32, 20133 Milano, Italy

[3] CNRS and Sorbonne Universités, UPMC Univ Paris 06, UMR 7190,
Institut Jean le Rond d'Alembert, 4 place Jussieu case 162, 75005 Paris, France

Keywords: branching instability, bacterial colony growth, pattern formation

Abstract

Self-organization in developing living organisms relies on the capability of cells to duplicate and perform a collective motion inside the surrounding environment. Chemical and mechanical interactions coordinate such a cooperative behavior, driving the dynamical evolution of the macroscopic system. In this work, we perform an analytical and computational analysis to study pattern formation during the spreading of an initially circular bacterial colony on a Petri dish. The continuous mathematical model addresses the growth and the chemotactic migration of the living monolayer, together with the diffusion and consumption of nutrients in the agar. The governing equations contain four dimensionless parameters, accounting for the interplay among the chemotactic response, the bacteria-substrate interaction and the experimental geometry. The spreading colony is found to be always linearly unstable to perturbations of the interface, whilst branching instability arises in finite-element numerical simulations. The typical length-scales of such fingers, which align in the radial direction and later undergo further branching, are controlled by the size parameters of the problem, whilst the emergence of branching is favored if the diffusion is dominant on the chemotaxis. The model is able to predict the experimental morphologies and their dynamical evolution, confirming that compact (resp. branched) patterns arise for fast (resp. slow) expanding colonies. Such results, while providing new insights on pattern selection in bacterial colonies, may finally have important applications for designing controlled patterns.

1 Introduction

The collective motion rather than the migration of single individuals is known to drive the macroscopic evolution of many biological processes, such as wound healing [1, 2], biofilm formation [3], tumor growth [1, 4–6], and morphogenetic processes [1, 7–9]. In fact, living cells and bacteria tend to form closely packed clusters (e.g. the columnar structures emerging in expanding living colonies) in which microscopic self-interactions result in cooperative migration [7, 10]. Although each individual in a population can determine its own fate, recent findings highlighted that single behaviors and abilities are adjusted, thanks to stochastic differentiation, in order to fit the needs of the population as a whole [11, 12].

In order to coordinate such cooperative activities, the chemical and the mechanical interactions both among individual entities and with the extracellular environment are of paramount importance. The chemical communication relies either on the cell capability of secreting chemicals (in cell-to-cell chemical signaling) or on the ability of sensing an external chemical field, by binding specific signal molecules through their membrane receptors [13]. The chemical interaction can occur between adjacent cells, but can also act over long distances, through complex intracellular mechanisms involving signal transduction networks and gene network dynamics [14]. Nevertheless, living matter is not only responding to soluble biochemical signals but also to physical factors,

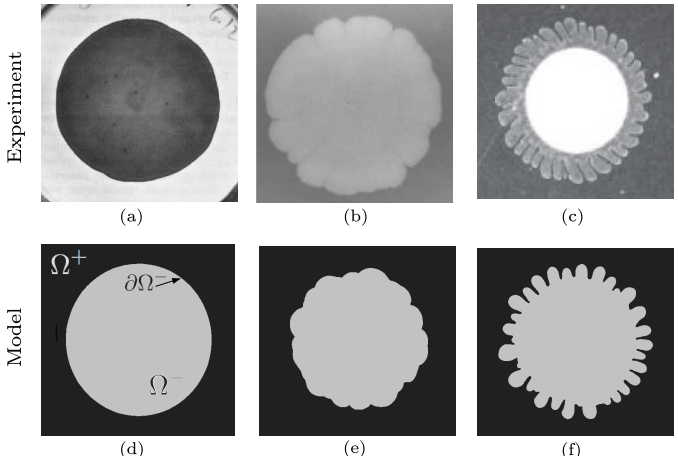

Figure 1: Comparison between some bacterial morphologies observed in biological experiments (top, a-c, reproduced with permission from [35], [23], [13] respectively) and the results obtained through the numerical simulations of the proposed mechanical model(bottom, d-f). The numerical simulations are obtained setting (d) $R_0^* = 31$, $R_{out} = 155$, $\beta = 160$ and $\sigma = 0.003$, (e) $R_0^* = 70$, $R_{out} = 350$, $\beta = 8.5$ and $\sigma = 0.007$, (f) $R_0^* = 100$, $R_{out} = 500$, $\beta = 1$ and $\sigma = 0.007$.

e.g. through surface cell receptors such as integrins and focal adhesion proteins, establishing a mechanical feedback of fundamental importance in both physiological and pathological conditions [15, 16]. Thus, endogenous and exogenous physical forces act as key regulators of important intracellular signals that drive the dynamical evolution of living organisms through mechano-transduction [17].

In particular, we focus here on pattern formation in expanding bacterial clusters, studying the influence of the chemotactic motility of the colony, the interaction between the bacteria and the substrate, as well as the size effects in experiments. A bacterial colony is an excellent biological system model to study general principles of collective motion and pattern formation in complex living organisms [10]. Furthermore, the study of cooperative migration and the onset of branched morphologies in bacterial colonies is an extremely multidisciplinary field of research, combining biological information with the mathematical theories of nonlinear dynamics and the physics and mechanics of non-equilibrium processes.

Thus, bacterial capability to develop elaborate branched patterns, even starting from an initially homogeneous microbial monolayer, has been intensively studied from the biological point of view, plating different bacterial colonies on a Petri dish covered with agar, under different environmental conditions [18–23]. Some of the observed patterns are reported in Fig. 1-top, ranging from disk-like colony (Fig. 1-a) to dense branched morphology (Fig. 1-c). These biological observations highlight that nutrient diffusion and the interaction with the substrate, together with the cellular capability to proliferate

and move either in a random-walk-like fashion or in response to an external chemical signals (i.e. chemotaxis), are the key ingredients in the progression of front instabilities.

Indeed, both the random and biased flagellation-based run-and-tumble bacterial motion, in conjunction with collective lubrication by secretion of surfactants, enables rapid colony expansion (up to centimeters per hour) [24] and it has been extensively studied for many bacterial species. However, for sake of completeness, we remark that some bacterial strains are able to colonize surfaces also using other motility mechanisms. In particular, recent works performed on Paenibacillus dendritiformis (morphotype C) [24] and on Myxobacteria [25] shows that very long bacterial cells will no longer swarm with the standard dynamic patterns of whirls and jets, but they rather form long tracks in which each individual bacteria periodically reverse their direction, moving back and forth along moderately curved lines [24, 25]. The time between switching in cell direction (which is approximately 20 s [24]) was found to be independent of the number of neighbors and of the environmental factors (e.g. the initial nutrient level, the surfactant additions, the agar rigidity, the humidity level and temperature), suggesting the existence of an extraordinary robust internal clock for reversal events in bacteria [24]. The evolutionary advantage of this unique back-and-forth motion remains unclear and deserves further studies [25]. In the following, we will not look in details at the modelling of the microscopic mechanisms generating the macroscopic motion, however the model we propose seems more suitable to describe standard run-and-tumble colony expansion.

Many in-silico mathematical models have been proposed to reproduce the spontaneous onset of the complex patterns observed during microbial growth. The theoretical approaches can be divided into two main categories: hybrid and continuous models. In hybrid models [18, 26–29] the microorganisms are represented as discrete, moving entities whereas the time evolution of the chemicals is described by reaction-diffusion equations. In continuous models [19, 22, 28, 30, 32, 33], the bacteria as well as the nutrients and all the other possible factors involved in the process are represented via their density per unit surface. The most popular models of bacterial growth are systems of reaction-diffusion equations [22, 23, 30, 32–34], that allow the description of colony patterns including not only spreading disk-like patterns, which was found to be consistent with the solution of a two-dimensional Fisher equation for the bacterial cell density [23, 34], but also branched ones. Since bacteria expansion is modeled only by diffusion (i.e. without allowance for chemotaxis), instabilities arise either because of a non-linear (e.g. density-dependent) diffusion coefficient [22, 32] or thanks to the introduction of a bacterial transition from the active-motile and proliferative state to a passive one [30]. Furthermore, the observed branched patterns have been recovered using the assumption of a nutrition limited process [19, 22, 32, 35, 36] or by combining signalling from a chemorepellent and a chemoattractant coupled with a proper dynamic for the colony, e.g. derived from the classical Keller-Segel model [37].

All of these researches focused on diffusing chemicals as the major driving factors of the process, neglecting any mechanical balance laws. Some efforts to include the mechanical considerations in the modelling of bacterial expansion during the colony

expansion have been done in hybrid models [27], having the major drawback of the small number of individuals that can be simulated numerically.
Moreover, the modelling of the viscous interaction between the colony and the substrate has been recently proposed in a continuous model of biofilm formation [3], proving the instability of a bacterial biofilm with planar front whose expansion relies on a nutrient-driven volumetric mass source without any chemotactic motion.
In this work, we investigate the growth and chemotactic mobility of a biological colony, coupled with the diffusion and consumption of nutrients provided by the agar, using a continuum mechanical model at the macroscopic scale. Since bacteria maintain the contact with their neighbors and no gaps appear during the culture expansion, the continuum assumption is effectively formulated. Moreover, bacterial growth within a Petri dish is described as a free-boundary two-dimensional problem. In the following, we first present the mathematical model based on thermo-mechanical considerations for describing the expansion of a circular bacterial colony. We later perform the linear stability analysis for the resulting diffusive circular growth and we study the dynamics of pattern formation in the nonlinear regime using numerical simulations.

2 Mathematical model

A bacterial colony can be modeled as a two-dimensional continuum body occupying a region denoted by Ω^-, with a moving boundary $\partial\Omega^-$ (see Fig. 1-d). The bacteria are immersed into a spatial outer domain, Ω^+, with boundary $\partial\Omega^+$, that stands for the border of the Petri-dish with radius R_{out}. The domain Ω^+ represents the lubricant fluid on the top of the agar, which seems to be collectively produced by the bacteria themselves, although it could also be drawn from the agar during the colony expansion [18, 19, 35].
The mathematical model takes into account the diffusion of the nutrients in the fluid on the top of the agar, the chemotactic mobility of the bacteria and the mechanical interactions with the substrate. Here, we will consider a single nutrient specie with volume concentration $n(\mathbf{x}, t)$, e.g. peptone, diffusing from the outer boundary $\partial\Omega^+$, with diffusion coefficient D_n and consumed, with an uptake rate γ_n, only in the region occupied by the living material, such that

$$\dot{n}(\mathbf{x}, t) = \begin{cases} D_n \nabla^2 n(\mathbf{x}, t) - \gamma_n n(\mathbf{x}, t) & \text{in } \Omega^- , \\ D_n \nabla^2 n(\mathbf{x}, t) & \text{in } \Omega^+ . \end{cases} \tag{1}$$

Considering that the living material can be macroscopically described by a Newtonian fluid moving at low Reynolds numbers [38–40], the classical Darcy's law gives the velocity of the living colony, $\mathbf{v} = -K_p \nabla p$, where K_p is the permeability coefficient describing the friction properties with the substrate and p is the pressure.
Then, assuming that the colony grows thanks to a non-convective mass flux $\mathbf{m}$, without any significant volumetric mass source, the standard mass balance for the bacterial spatial density ρ reads $\partial\rho/\partial t + \nabla \cdot (\rho \mathbf{v}) = \nabla \cdot \mathbf{m}$. Being bacteria mostly composed by

water, the incompressibility constraint leads to $\rho\nabla\cdot\mathbf{v}=\nabla\cdot\mathbf{m}$.
Biological evidences suggests that bacteria are able to implement directional movements, by decreasing the tumbling frequency of their flagella, when they move up the gradient of the chemo-attractant [41]. Thus, neglecting the random-motion of bacteria with respect to the directional one, we can assume that the non-convective mass flux vector is directed along the gradient of the chemical concentration, such that $\mathbf{m}=\chi\rho\nabla n$, where χ is the chemotactic coefficient [37]. Substituting the Darcy's law in the mass balance equation for a homogeneous microbial colony gives the following relation between the pressure p and the nutrient concentration:

$$\nabla^2 p=-\frac{\chi}{K_p}\nabla^2 n \quad \text{in } \Omega^- \,. \tag{2}$$

In order to solve the system of partial differential equations (5)-(2), boundary conditions are to be provided. In particular, on $\partial\Omega^-$, we apply the Young-Laplace equation for the pressure, the compatibility condition for the moving interface and the classical continuity conditions for the nutrient concentration and its normal derivative

$$p=p_0-\sigma_b C\,, \quad \frac{\mathrm{d}\mathbf{x}_{\partial\Omega^-}}{\mathrm{d}t}\cdot\mathbf{n}=\mathbf{v}_{\partial\Omega^-}\cdot\mathbf{n}\,, \tag{3}$$

$$[\![n]\!]|_{\partial\Omega^-}=0\,, \quad [\![\nabla n\cdot\mathbf{n}]\!]|_{\partial\Omega^-}=0\,, \tag{4}$$

where C is the local curvature of the free boundary, σ_b the surface tension of the interface, p_0 the constant outer pressure and $\mathbf{n}$ the outward normal vector at the boundary. It is worth noticing that the surface tension of the bacterial colony results from the collective interaction with the biopolymers forming the surrounding liquid environment [42]. In the following we will apply this model to a initially circular bacterial colony of radius $R_0^*=R^*(t=0)$, and we will use the non-dimensional system of equations for the dimensionless chemical concentration, $\bar{n}$, and the dimensionless pressure, $\bar{p}$

$$\dot{\bar{n}}=\begin{cases}\nabla^2\bar{n}-\bar{n} & \text{in } \Omega^-\\ \nabla^2\bar{n} & \text{in } \Omega^+\end{cases} \tag{5}$$

$$\nabla^2\bar{p}=-\beta\nabla^2\bar{n} \quad \text{in } \Omega^- \tag{6}$$

that has been obtained, taking the following characteristic time t_c, length l_c, velocity v_c, pressure p_c and chemical concentration n_c: $t_c=\gamma_n^{-1}\,, l_c=\sqrt{D_n\gamma_n^{-1}}\,, v_c=\sqrt{D_n\gamma_n}$, $p_c=D_nK_p^{-1}$, $n_c=n|_{R_{out}}$, where $n|_{R_{out}}$ is the fixed concentration at the outer border of the Petri dish. In dimensionless form, the boundary conditions for the pressure, the chemical concentration of the nutrients and the velocity, on the colony front $\partial\Omega^-$, read

$$\bar{p}=\bar{p}_0-\bar{\sigma}\bar{C} \tag{7}$$

$$[\![\bar{n}]\!]|_{\partial\Omega^-}=0\,, \quad [\![\nabla\bar{n}\cdot\mathbf{n}]\!]|_{\partial\Omega^-}=0 \tag{8}$$

$$\frac{\mathrm{d}\bar{\mathbf{x}}_{\partial\Omega^-}}{\mathrm{d}t}\cdot\mathbf{n}=\bar{\mathbf{v}}_{\partial\Omega^-}\cdot\mathbf{n}\,. \tag{9}$$

On the other hand, on $\partial\Omega^+$, the boundary condition on the nutrient concentration, is $\bar{n}(t, R_{out}) = 1$.
In the following we will omit the barred notation to denote dimensionless quantities, for sake of simplicity.
The nondimensionalization procedure (see the Supplementary Material for further details) leads to the definition of four dimensionless parameters: two of them, $\beta := \chi n_c/D_n$ and $\sigma := \sigma_b K_p \gamma_n^{1/2} D_n^{-3/2}$ are related to the chemotactic response and the bacteria-substrate interaction (*motility* parameters), whereas the other two, R_0^* (i.e. dimensionless initial radius of the circular colony) and R_{out} (i.e. the dimensionless outer radius of the Petri dish) define the geometrical properties of the system with respect to the diffusive length, l_c (*size* parameters). In particular, the dimensionless parameter β represents the ratio between the energy required for the chemotactic expansion of the colony and the energy provided by the diffusive nutrients, whereas, considering that K_p can be related to the friction between the colony and the substrate, ζ, through $K_p = l_c/\zeta$, the dimensionless parameter σ becomes the ratio between the surface tension of the bacterial colony and the product of the colony-substrate friction and the diffusion coefficient, i.e. $\sigma = \sigma_b/(D_n\zeta)$.

3 Results

3.1 Linear stability analysis

Usually, the linear stability analysis for problems with a moving interface is performed around a steady state (when present) or around a steady wave profile in a comoving frame. However, in our particular case, it is neither possible to find a traveling wave solution, being the domain finite, nor finding a steady-state solution for the bacterial front. Thus, in order to perform some analytical calculations, let us consider the quasi-stationary expansion of a circular bacterial colony of radius $R^*(t)$, assuming that the diffusive process is much faster than the border expansion, so that the time-derivative term in (5) can be neglected. The quasi-stationary velocity of the circular front has only a radial component, i.e. $\mathbf{v}^* = v_r^* \mathbf{e}_r$, with $v_r^* = \beta n_0 I_1(R^*)/I_0(R^*)$, where $I_j(r)$ is the modified Bessel function of the first kind of order j, evaluated in r, and $n_0 = (1 + I_1(R^*)/I_0(R^*) R^* \log(R_{out}/R^*))^{-1}$ is the nutrient concentration at the free boundary, in the quasi-stationary state. More details on the derivation of the quasi-stationary solution are presented in the Supplementary Materials.
Considering a perturbation of the moving interface given by $R(\theta, t) = R^*(t) + \varepsilon e^{\lambda t + ik\theta}$, it is possible to find the dispersion equation relating the time growth rate λ to the integer wave-number k in an implicit way, as a function of the four dimensionless parameters β, σ, R^* and R_{out}:

$$\lambda = -\frac{\sigma}{{R^*}^3}(k^3 - k) + \beta A_\lambda \sqrt{\lambda + 1} I_{k+1}(\sqrt{\lambda + 1} R^*) - \beta n_0 \left((1 + k) \frac{I_1(R^*)}{R^* I_0(R^*)} - 1 \right), \quad (10)$$

for $\lambda \neq -1$. More information on the procedure used to obtain the dispersion relations and the determination of the coefficient A_λ can be found in the Supplementary Mate-

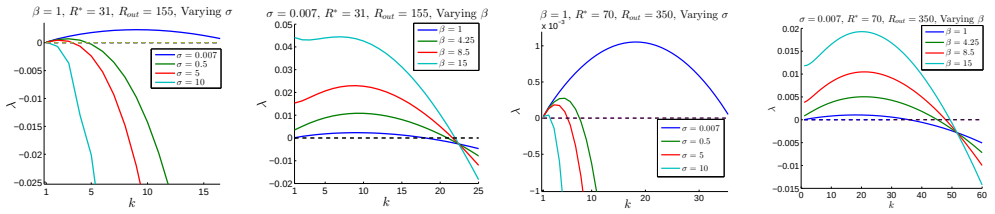

(a) (b) (c) (d)

Figure 2: Dispersion diagrams, varying (a)-(c) σ and (b)-(d) β, for a colony of radius $R^* = 31$ in a Petri dish of radius $R_{out} = 155$ in (a) and (b) and a colony of radius $R^* = 70$ in a Petri dish of radius $R_{out} = 350$ in (c) and (d). Solid lines correspond to the interpolation of values of λ obtained for the integer values $k \geq 1$, $k \in \mathbb{N}^+$, through numerical solution of the dispersion equations (10).

rial.

Interestingly, eq. (10) shows that the amplification rate of the perturbation depends on the radius of the colony, R^*. The dispersion diagrams presented in Fig. 2, obtained iteratively solving the dispersion equation (10) through the secant method, demonstrates that the colony boundary is always linearly unstable for large wavelengths. The resulting dispersion curves show a stabilization of the front at short-wavelengths, which is also typically found in some classical fluid instabilities [43]. Indeed, the governing equations closely resemble to the ones driving the Saffman-Taylor instability in a Hele-Shaw cell, where σ has the same physical meaning of the capillary number, introducing a correction in the dispersion relation proportional to $(-k^3 + k)$ [44]. Such a regularizing effect is even enforced in our model by the presence of the laplacian operator at the right-hand side of Eq. 2, corresponding to a mass source term which is not considered in viscous instabilities. Whilst for a planar front one would expect to find $\lambda = 0$ for $k = 0$ for translational symmetry, we must remind that for the circular front we consider $k \in \mathbb{N}^+$, since $k = 0$ would correspond to the quasi-static expansion of the circular front. Furthermore, even if β somewhat physically corresponds to the influx volume flow rate in an initially circular front, the velocity of the quasi-stationary front depends in this problem on the initial radius R^* whilst it is often taken as a constant in viscous fingering problems [45], thus introducing a marked size-dependence in the resulting dispersion equation. In both cases the linear stability analysis can identify the finite critical wavelength with most unstable growth rate, which also increases for increasing β. Nonetheless, even if such linear stability curves are indicative of an unstable front dynamics, suggesting the nonlinear formation of dendritic patterns [46], we also expect to find differences in the fully nonlinear dynamics due to the more complex functional dependence on the growth and geometrical parameters in this probem. Furthermore, the maximum time growth rate increases as far as β increases, as shown in Fig. 2-b-d. Comparing the dispersion curve for different dimensionless radii of the colony, maintaining the ratio between R^* and tR_{out} constant (which will correspond

to different diffusive length), it is possible to see that, as the size parameters increases the range of unstable wavenumber increases but the maximum time growth rate of such instabilities is slower (Fig. 2-b vs. Fig. 2-d).
Furthermore, the dispersion diagrams in Fig. 2 highlights the existence of a characteristic wavenumber in the development of instabilities, that increases for bigger size parameters (Fig. 2-b vs. Fig. 2-d).

3.2 Numerical simulations

Since the linear analysis indicates the occurrence of a front instability with a characteristic wavenumber, we investigate the non-linear pattern formation of the bacterial colony using a finite element code implemented in FreeFem++ [48]. The equations (5)-(2) are solved on an adaptively refined triangular grid, fitting the moving interface. Given the concentration of nutrients at time t_i, we first compute the pressure p_i, through eq. (2) and then the velocity field, using the Darcy's law. We are yet able to explicitly move the boundary and solve (5) for the concentration at time t_{i+1}, using an implicit-Euler scheme.
The numerical results are reported in Figure 3-a showing the emerging patterns versus the two dimensionless parameters β and R_{out}, at fixed R_{out}/R_0^* and σ.
In particular, it is found that the branching of the colony is strongly favored by smaller values of the motility parameter β. Since β drives the velocity of the quasi-stationary front, we find that the contour instability is enhanced by a low expanding velocity, which is a common feature of growing biological systems in a diffusion dominated regime [5]. In fact, small values of β correspond to situations in which the diffusion of chemicals is dominant on the chemotactic mobility of the colony.
Furthermore, Fig. 3-a points out the existence of a size effect in pattern formation, showing that the size parameter R_{out} determines the characteristic wavelength of the branching process. In fact, keeping the aspect ratio R_{out}/R_0^* constant, a larger size of the Petri dish R_{out}, with respect to the diffusive length l_c, determines branched patterns characterized by a smaller wavenumber.
The morphological diagram in Fig. 3-a also confirms the results obtained with the linear stability analysis of the quasi-stationary problem. Indeed, the blue dispersion curves in Fig. 2-a-b predicts, for the particular case $\beta = 1$, $R_0^* = 31$ and $R_{out} = 155$, a characteristic branching wavenumber, $9 \leq k_c \leq 10$ and in the numerical simulations (see Fig. 3-a top-right) we have ten totally developed branches. On the other hand, for $\beta = 1$, $R_0^* = 70$ and $R_{out} = 350$, the analytical characteristic wavenumber (see the blue dispersion curves in Fig. 2-c-d) is $18 \leq k_c \leq 19$, which is confirmed by the numerical simulation in Fig. 3-a bottom-right, where nineteen totally developed branches appear. Considering $\beta = 4.25$, the maximum in the red dispersion curve in Fig. 2-d shifts to $21 \leq k_c \leq 22$, which is in agreement with the twenty-two fingers that develop in Fig. 3-a bottom-center, where the same parameters are considered. The agreement between numerical and analytical results is valid as long as the velocity of the front is slow enough in order to satisfy the quasi-stationary hypothesis. Thus, for high values of the parameter β, that leads to a fast front dynamic, non-linear effects stabilize the

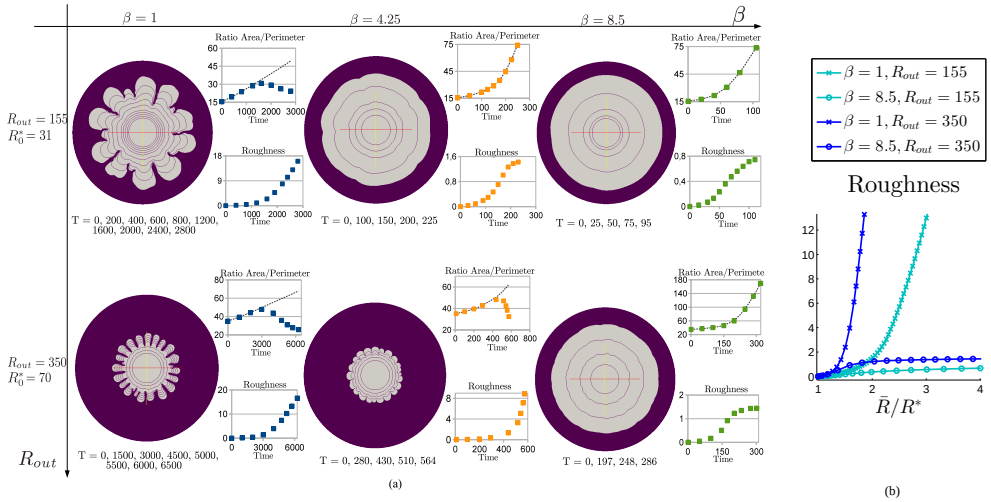

Figure 3: Morphological diagram of the expanding bacterial colony for different values of β and R_{out} in the numerical simulations, setting $\sigma = 0.007$ and $R_{out}/R_0^* = 5$ fixed. (a) The contour of the colony is plotted at different instants of time. The top-right charts report the area/perimeter ratio of the bacterial colony (square markers) and half of the averaged radius of the colony (dashed lines), whereas the bottom-right charts depict the roughness of the interface over time. (b) Roughness of the colony contour for different values of the parameters β and R_{out}, over the normalized averaged radius of the colony. Branched patterns show a continuously increasing roughness, which in turn saturates for rounder colonies. The dynamic plots of the chemical concentration and the pressure fields are reported in the Movie 1 and Movie 2 of the Supplementary Material, for the particular case $\beta = 1$, $R_{out} = 155$, $R_0^* = 31$.

evolution of the colony profile.

The morphological diagram in Fig. 3-a also highlights that the occurrence of branching can be detected when the ratio between the area of the colony and its perimeter over time (square markers) deviates from the half of the average radius of the colony (dashed lines).

Another important parameter in the definition of branched patterns is the roughness of the profile, measured as the root of the mean square deviation of points on the front from the average radius of the colony [28]. Either plotting this parameter as a function of time (see Fig. 3-a) or as a function of the averaged radius of the colony, $\bar{R}$, normalized with respect to the initial radius, R_0^* (Fig. 3-b), it is possible to observe that the interface roughness continuously increases for branched patterns, whereas it later saturates to an almost constant value only in compact colonies, in agreement with the experimental measurements performed in [49]. In summary, it is found that the motility parameter β defines the occurrence of the branching regime, whereas, the size parameter R_{out} determines the characteristic wavelength of the branching process.

Furthermore, numerical simulations agree with the theory in predicting that an increase

of the surface tension σ has a stabilizing effect also in the non-linear regime (see Fig. 4-a and Movie 3, Movie 4 and Movie 5 in the Supplementary Material). Another important parameter in the model is the initial size of the colony, with respect to the diffusive length, R_0^*. In order to assess the influence of this parameter on the onset of branches, we run a set of simulations, keeping R_{out}, σ and β fixed and letting R_0^* vary. The morphological diagram reported in Fig. 4-b shows that, as the radius of the colony increases, an higher number of fingers develops.

Let us now briefly discuss the characteristics of the branching process in the expanding colony. Once branching has been triggered, all developing fingers elongate in the radial direction. Further branching can occur, even though some of the second generation fingers remain very short, because of the geometrical constraint imposed by their neighbors. In Fig. 5 the geometrical characteristics of the finger are plotted versus time. We define the finger base, B, as the distance between two subsequent points of local maximum for the curvature of the moving front. The amplitude of the finger, A, is defined as the maximum distance between the points belonging to the finger contour and the corresponding finger base segment. The numerical results in Fig. 5 correspond to the simulation on the upper-left of Fig. 3. It is observed that at an early stage (up to $t = 1650$) both the amplitude and the base strongly increase for each of the five evolving fingers. As soon as second generation fingers appear (from $t = 1650$ on), the amplitude of the new ones strongly increases, whereas the base remains almost constant in time. We report in the Table within Fig. 5 the parameters of the power-law curve, $c \cdot t^{\alpha}$, which best fits the numerical data for the base and the amplitude of the fingers. Interestingly, at the early stage the best fitting exponent for the ratio amplitude/base of the fingers is ≈ 0.45, which is very close to the expected square root growth over time exponent in a diffusion-driven instability [43].

Let us now return to the dimensional physical quantities in order to discuss the results of the numerical simulations with respect to the biological data. Available data in experimental literature for expanding colonies are shown in Table 1. In particular, in the following, we compare the results of the simulated patterns of our model, reported in Fig. 1(bottom), with their corresponding experimental counterparts in Fig. 1(top). In all cases, the Petri dishes in experiments have the standard radius of $44\,\mathrm{mm}$.

As shown in Figure 1-d, the evolution of the disk-like colony observed in [35] can be reproduced by taking a diffusion coefficient $D_n = 3 \cdot 10^{-11}\,\mathrm{m}^2/\mathrm{s}$, and a small uptake rate, $\gamma = 3.7 \cdot 10^{-4}\,\mathrm{s}^{-1}$, giving a characteristic length $l_c \approx 285\,\mu\mathrm{m}$, corresponding to a dimensionless external radius of $R_{out} \approx 155$. Fixing $\beta = 8.5$ we obtain an average velocity of the front equal to $\approx 3.2\,\mathrm{mm/h}$, which is in the order of magnitude of the values found in literature for round and compact colonies, such as the one in Fig. 1-a (see Table 1). Considering the characteristic concentration $c_n = 0.1\,\mathrm{mM}$, as the one used in [50], the parameter $\beta = 8.5$ describes a chemotactic coefficient $\chi \approx 48 \cdot 10^{-5}\,\mathrm{cm}^2/(\mathrm{s} \cdot \mathrm{mM})$, which is also in the biological range (see Table 1).

Thus, disk-like patterns are found to arise in situations in which the chemicals have an intermediate diffusion rate and are consumed by bacteria at a slow rate. Moreover, an Eden-like pattern (i.e. a clusters whose inner structure is almost completely compact but whose surface is comparatively rough [23]) is observed considering a smaller dif-

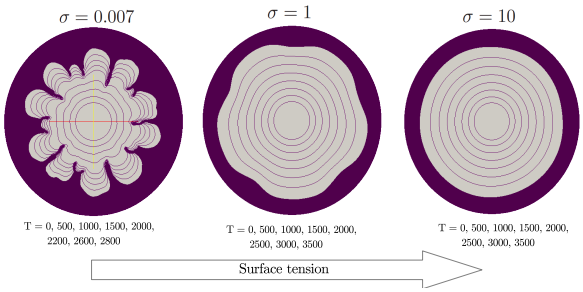

(a)

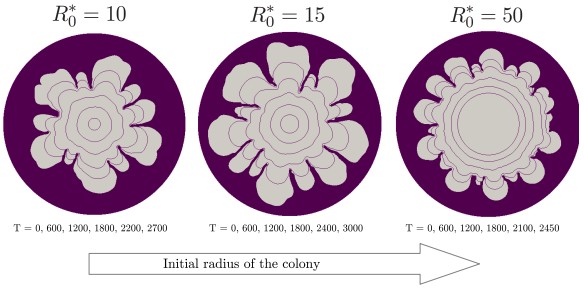

(b)

Figure 4: Influence of a) the parameter σ and b) the initial radius R_0^* on the formation of contour instabilities. a) The surface tension has a stabilizing effect on the motion of the free boundary. The simulations were obtained imposing $R_{out} = 155$, $R_0^* = 31$ and $\beta = 1$. The dynamic plots of the contours are reported in the Movies 3, 4 and 5 of the Supplementary Material. b) The number of fingers that develops increases as the radius of the colony is bigger. The simulations were obtained imposing $R_{out} = 155$, $\sigma = 0.007$ and $\beta = 1$.

fusion coefficient $D_n = 10^{-11}\,\mathrm{m}^2/\mathrm{s}$ [35] and an uptake rate $\gamma = 6.5 \cdot 10^{-4}\,\mathrm{s}^{-1}$ (i.e. $l_c \approx 124\,\mu\mathrm{m}$ and $v_c \approx 290\,\mu\mathrm{m/h}$, $R_{out} \approx 350$) as depicted in Fig. 1-e. Keeping $\beta = 8.5$, the resulting mean front velocity is equal to $136\,\mu\mathrm{m/h}$, which is in agreement with the reported velocities for such patterns (see Table 1). In this case, under the same assumptions used above, we obtain a consistent chemotactic coefficient of about $\chi \approx 0.85 \cdot 10^{-5}\,\mathrm{cm}^2/(\mathrm{s} \cdot \mathrm{mM})$. Therefore, our model predicts that Eden-like structures can be obtained in the range of relatively small diffusion coefficient of the nutrients, intermediate uptake rates and small chemotactic behaviour. However, for sake of completeness, we have to remark that, even though the model is able to reproduce the "fusion" of really thick branches leading to a macroscopic roughness of a compact colony, as observed in Eden-like patterns, it is not possible to reproduce the observe microscopic roughness [30], as smaller wavelengths are stabilize.
Furthermore, we have found that branched structures arise in simulations with high values of the dimensionless external radius R_{out} and small values of the motility parameter β, physically corresponding to high values of both nutrient diffusion and uptake rate,

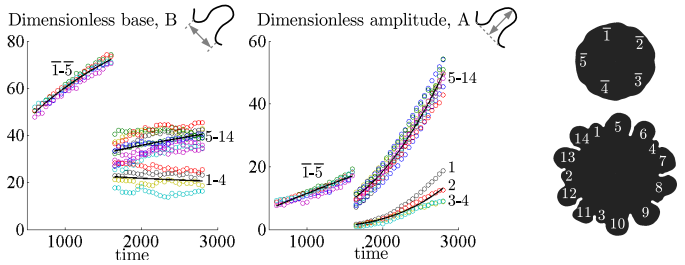

(a) (b)

Fit. ct^α	c	α
B ($\bar{1}$-$\bar{5}$)	4.18	0.386
A ($\bar{1}$-$\bar{5}$)	0.036	0.83
B (1-14)	71.2 (1-4); 2.3 (5-14)	-0.16 (1-4); 0.36 (5-14)
A (1-14)	1.9e-13 (1-4); 3e-09 (5-14)	4.0 (1-4); 2.9 (5-14)

(c)

Figure 5: Fingers' base and amplitude in the case $\beta = 1$, $R_{out} = 155$, $R_0^* = 31$, $\sigma = 0.007$. (a) Base and amplitude of fingers (circles): up to time $t = 1650$, five principal fingers develop, then tip splitting occurs and 14 fingers emerge. (b) Numbering of the fingers considered in the simulation. (c) Table reporting the fitting parameters of the data with a power-law curve of the kind ct^α (solid lines).

coupled with low concentration of nutrients in the agar. Indeed, the fingers' development and evolution reported in [13] are reproduced by our simulations in Fig. 1-f, considering $\gamma = 0.11 s^{-1}$ and $D_n = 10^{-10}\,\mathrm{m}^2/\mathrm{s}$, so that $l_c \approx 30\,\mu\mathrm{m}$ and $t_c \approx 9\,\mathrm{s}$. Accordingly, the observed displacement of about $2.4\,\mathrm{mm}$ in the first 22 hours, for an initial colony with a diameter of about $6\,\mathrm{mm}$ [13], perfectly corresponds to the displacement of the front recorded in this simulation (i.e. $82 \cdot l_c$ at $T = 9000$, for a colony with $R_0^* = 100$). In this case we fix $\beta = 1$, corresponding to a chemotactic coefficient $\chi \approx 10^{-5}\,\mathrm{cm}^2/(\mathrm{s} \cdot \mathrm{mM})$, which is slightly below the typical values reported in [50].
In summary, our model is able to predict the observed experimental morphologies, reproducing that higher velocities of the front, which are linked to a stronger response of bacteria to the external chemical field (i.e. high χ), correspond to more rounded profiles, in accordance to biological observations [22, 30].
Let us finally add few considerations about the role of surface tension for pattern formation. Considering a friction coefficient $\zeta = 1\,\mathrm{nNs}/(\mu\mathrm{m})$ (compatible with the values reported in Table 1), the surface tension for the three simulations results in the range $\sigma_b \approx 0.09 - 0.7\,\mathrm{nN}/\mu\mathrm{m}$, which is slightly higher than the values found for cell clusters (see Table 1). Accordingly, although we find that disk-like colonies can also be numerically obtained by increasing the dimensionless motility parameter σ (see Fig. 4), this would correspond to values of the surface tension much higher than the biologically range. In conclusion, we argue that the compact expansion of the bacterial front likely relies more on the capability of bacteria to actively move and consume nutrients and on

the diffusive properties of the chemicals in the agar, rather than on the surface tension and the adhesive properties of the colony.

Table 1: Biologically meaningful ranges for the parameters of the model.

	Values	Ref.
D_n	$10^{-11} - 10^{-9}\,\mathrm{m}^2/\mathrm{s}$	[3,35,50,51]
γ_n	$10^{-4} - 10^{-3}\,\mathrm{s}^{-1}$	[52]
v_{colony}	$60 - 400\,\mu\mathrm{m/h}$ (finger);	[13,22]
	$60 - 300\,\mu\mathrm{m/h}$ (Eden); $4 - 18\,\mathrm{mm/h}$ (disk)	[22,30]
σ_b	$0.07\,\mathrm{nN}/\mu\mathrm{m}$	[53]
ζ	$1 - 10^2\,\mathrm{nNs}/(\mu\mathrm{m}^3)$	[54]
χ	$3.75 - 188 \cdot 10^{-5}\,\mathrm{cm}^2/(\mathrm{s}\cdot\mathrm{mM})$	[50,55]

4 Discussion

In this work we have presented an analytical and computational analysis of a continuum model for studying pattern formation during the spreading of an initially circular bacterial colony on a Petri dish. The proposed model differs from previous ones [3,23,32] for taking into account both the chemical effects, dictated by the diffusion of nutrients and the chemotactic response of bacteria and the mechanical/viscous interaction between the colony and the substrate. In particular, four dimensionless parameters are found to characterize the model dynamics: two of them describe the factors which drive the *motility* of the colony, i.e. β represents the competition between chemotactic and diffusive effects, whereas σ is the ratio between the surface tension of the colony and the friction with the substrate, whilst the initial dimensionless radius of the colony, R_0^*, and the dimensionless radius of the Petri dish, R_{out}, account for *size* effects.

The linear stability analysis has evidenced that an initially circular colony is always linearly unstable to perturbations of the interface, having the typical dispersion curves found for fluid instabilities, such as viscous fingering. The numerical simulations of the bacterial spreading in the fully nonlinear regime have confirmed the development of undulated finger-like structures, which align in the radial direction and later undergo further branching, and the existence of characteristic wavenumber, as predicted by the linear stability analysis. Whilst the finger dynamical behaviour show the occurrence of the typical shielding and tip-splitting found in Saffman-Taylor instability [44], we find here a more complex dependence of the typical length-scales of such fingers on the size parameters of the problem, with more branched patterns appearing with larger Petri dishes, whilst the emergence of branching is driven by the motility parameters, being especially favored by small values of σ and β. However, through comparison of the model parameters with real biological data, we argue that the selection mechanism of branched patterns likely relies on the *motility* parameter β, i.e. on the interplay between diffusion and chemotaxis, rather than on σ. In particular, in such a range, the

aspect ratio of the fingers is found to scale as about the square root of the time. Since β drives the velocity of the colony interface, the model also confirms the experimental observations that compact (resp. branched) patterns arise for fast (resp. slow) expanding colonies [22, 30]. Furthermore, the scaling laws for the roughness coefficient of the interface in numerical simulations are consistent with the ones reported in the biological investigations [34].

Interestingly, the modeling of the branching structures does not require neither the introduction of a non-linear (e.g. density-dependent) diffusion coefficient, as in [22, 32, 56], nor the transition from the active-motile and proliferative state of bacteria to a passive state, as in [30].

The experimental morphologies reported in [13, 23, 35] (Fig. 1, top) are also compared with the patterns resulting from the numerical simulations of the proposed model (Fig 1, bottom), where the relevant biological parameters in each experimental setting are used as input. A striking similarity has been found between experiments and model simulations either on the emerging disk-like, Eden-like and branched structures, or on the pattern dynamics during the expansion process.

Even though coupling smaller values of the parameter β with bigger size parameters, will lead to an increased number of first and second generation fingers, the model presented seems not able to reproduce the evolution of colonies in which fractal patterns or a microscopic roughness appears, due to the stabilization of really small wavelengths. Highly fractal patterns are more easily reproducible either using reaction-diffusion models with non-linear terms [31, 32, 35], where an explicit representation of the interface with associated continuous mechanical quantities is not present, or with discrete/hybrid models (with the obvious limitations) [18, 28]. Thus, the model proposed is limited to those situations in which the assumptions under which it has been derived hold and it cannot be applied to describe the occurrence of patterns where a continuous representation of the colony is not possible, as the typical structure dimension is of the order of a single cell.

In conclusion, the results of this study suggest that the pattern selection and evolution in expanding bacterial colonies is driven by a complex interplay of the chemotactic response, the substrate-bacteria interaction and the size effects. Furthermore, the present study highlights the necessity to perform new experimental tests with a better quantitative characterization of both the chemical response and the mechanical forces involved during the bacterial expansion, as done for eukaryotic cells [57, 58]. Indeed, even if the formation of spatial patterns in growing bacterial colonies has been intensely studied during the last years, further progress on the field has been hindered by the lack of detailed experimental data [10]. Such a combined approach has the potential to foster our understanding of the pattern selection and dynamics in bacterial colonies, with important applications for designing and engineering controlled patterns.

Future works will be focused on one hand, on the refinement of the proposed model, simulating more realistic initial and boundary conditions, possibly supported by biological experiments, coupled with a more complex representation for the living material (e.g. viscoelastic) and on a rigorous representation of the active motility and the chemo-mechanical interactions occurring at the microscopic scale inside the colony,

which are of fundamental importance in the appearance and evolution of certain bacterial strains [10, 24, 25].
On the other hand, it might be interesting to study the application of this model, with proper modifications, to free-boundary problems in other biological systems (e.g. wound healing), aiming at giving insights on the role played by physical forces in directing self-organization in developing living organisms.

Acknowledgment

This work was partially supported by the "Start-up Packages and PhD Program" project, co-funded by Regione Lombardia through the "Fondo per lo sviluppo e la coesione 2007-2013 -formerly FAS" and by the "Progetto Giovani GNFM 2014", funded by the National Group of Mathematical Physics (GNFM-INdAM). We are grateful to Davide Ambrosi for helpful discussions.

Supplementary Material

S1. Linear Stability analysis

In this section we analytically study the stability of the quasi-stationary condition of the proposed model. The quasi-stationary problem is obtained assuming that in the first stages of colony incubation, the diffusive process is faster than the expansion of the front, so that a stationary condition for the nutrient concentration is reached before bacteria start proliferating and $\dot{n} \approx 0$. We consider a circular bacterial front, positioned in a Petri dish, thus $\Omega^- = \{(r,\theta) : r \leq R^*(t), 0 < \theta \leq 2\pi\}$ and $\Omega^+ = \{(r,\theta) : R^*(t) < r \leq R_{out}, 0 < \theta \leq 2\pi\}$ where $R^*(t)$ is the dimensionless radial position of the free boundary of the colony and R_{out} is the external boundary.

S1.1. Quasi-stationary solution

Imposing the boundary conditions (8), the stationary solution of eq. (5), denoted with n^*, is

$$n^*(r,t) = \begin{cases} n_0 \dfrac{I_0(r)}{I_0(R^*)} & \text{if } r < R^* \\ n_0 + (1-n_0)\dfrac{\log\left(\dfrac{r}{R^*}\right)}{\log\left(\dfrac{R_{out}}{R^*}\right)} & \text{if } R^* < r \leq R_{out}, \end{cases} \tag{11}$$

where $n_0 = n_0(t) = \left(1 + \dfrac{I_1(R^*)}{I_0(R^*(t))} R^*(t) \log\left(\dfrac{R_{out}}{R^*(t)}\right)\right)^{-1}$ is the concentration of the nutrient at the free boundary, located in R^* and $I_j(r)$ is the modified Bessel function

of the first kind of order j evaluated in r. Once this quasi-stationary concentration of the nutrient is known it is possible to solve (6), which leads to

$$p^*(r,t) = -\beta\left(n^*(r,t) - n_0\right) + p_0 + \frac{\sigma}{R^*}\,, \tag{12}$$

given that the pressure should be bounded and the Laplace condition (7) should hold. The quasi-stationary velocity of the front is directed along the radial direction, $\mathbf{v}^* = v_r^*\mathbf{e}_r$, with

$$v_r^*(R^*) = \beta n_0 \frac{I_1(R^*)}{I_0(R^*)}\,. \tag{13}$$

Therefore the quasi-stationary velocity of the front does not depend on the permeability coefficient, K_p, but it only relies on the position of the front and on the parameters characterizing the mass flux and the diffusive process of the nutrient.

S1.2. Perturbation of the quasi-stationary solution

We consider a perturbation of the free-boundary, of the kind

$$R(\theta,t) = R^*(t) + \varepsilon e^{\lambda t + ik\theta} \tag{14}$$

where λ is the amplification rate of the perturbation and k is the spatial wave-number. Then the variation of n and p from the quasi-stationary solution, n^* and p^* can be expressed as

$$n(r,\theta,t) = n^*(r,t) + \varepsilon n_1(r) e^{\lambda t + ik\theta}\,, \tag{15}$$

$$p(r,\theta,t) = p^*(r,t) + \varepsilon p_1(r) e^{\lambda t + ik\theta}\,. \tag{16}$$

From eq. (2.5), n_1 is the solution of the following ODE,

$$r^2 n_1''(r) + r n_1'(r) - \left(k^2 + (\lambda + H(R^* - r))r^2\right) n_1(r) = 0 \tag{17}$$

where $H(R^*-r) = 1$ if $r \le R^*$, whereas $H(R^*-r) = 0$ if $R^* < r \le R_{out}$ and primes denote derivative on r. In the following we will use the notations n_1^- and n_1^+ for the solution of the perturbed concentration for $r \le R^*$ and $R^* < r \le R_{out}$ respectively. The nature of the solution of (17) depends on the parameter λ, in particular

- for $\lambda \neq \{0, -1\}$: $n_1^-(r) = AI_k(\sqrt{\lambda+1}r)$ and $n_1^+(r) = CI_k(\sqrt{\lambda}r) + DK_k(\sqrt{\lambda}r)$;
- for $\lambda = 0$: $n_1^-(r) = A_0 I_k(\sqrt{\lambda+1}r)$ and $n_1^+(r) = C_0 r^k + D_0 r^{-k}$;
- for $\lambda = -1$: $n_1^-(r) = A_1 r^k$ and $n_1^+(r) = C_1 I_k(\sqrt{\lambda}r) + D_1 K_k(\sqrt{\lambda}r)$,

where $K_j(r)$ is the modified Bessel function of the second kind of order j, evaluated in r. The coefficient $A, C, D, A_0, C_0, D_0, E_0, A_1, C_1, D_1, E_1$ can be easily determined

Table 2: Solution of the perturbed pressure and implicit expression of the dispersion equations, for $\lambda \neq -1$.

Perturbed pressure	$p_1(r) = Er^k - \beta A_\lambda I_k(\sqrt{\lambda+1}r)$ $E = \frac{1}{R^{*k}}\left(\frac{\sigma}{R^{*2}}(k^2-1) + \beta n_0 \frac{I_1(R^*)}{I_0(R^*)} + \beta A_\lambda I_k(\sqrt{\lambda+1}R^*)\right)$
Dispersion equation	$\lambda = -\frac{\sigma}{R^{*3}}k(k^2-1) + \beta A_\lambda \sqrt{\lambda+1} I_{k+1}(\sqrt{\lambda+1}R^*) +$ $-\beta n_0\left((1+k)\frac{I_1(R^*)}{R^* I_0(R^*)} - 1\right)$ $A_\lambda = n_0 \frac{I_k(\sqrt{\lambda}R^*)K_k(\sqrt{\lambda}R_{out}) - K_k(\sqrt{\lambda}R^*)I_k(\sqrt{\lambda}R_{out})}{denA_\lambda}$ $denA_\lambda = \sqrt{\lambda+1}I_{k-1}(\sqrt{\lambda+1}R^*)\left(I_k(\sqrt{\lambda}R_{out})K_k(\sqrt{\lambda}R^*) - K_k(\sqrt{\lambda}R_{out})I_k(\sqrt{\lambda}R^*)\right) +$ $+\sqrt{\lambda}I_k(\sqrt{\lambda+1}R^*)\left(I_k(\sqrt{\lambda}R_{out})K_{k-1}(\sqrt{\lambda}R^*) + K_k(\sqrt{\lambda}R_{out})I_{k-1}(\sqrt{\lambda}R^*)\right)$

imposing the boundary conditions (2.8), which lead to the following set of boundary conditions for n_1

$$n_1(R_{out}) = 0 \tag{18}$$

$$[\![n_1]\!]|_{R^*} = 0 \tag{19}$$

$$[\![\frac{\partial n_1}{\partial r}]\!]|_{R^*} = n_0\,. \tag{20}$$

Once that n_1^- is known it is possible to determine p_1. From eq. (2.6), we obtain

$$p_1(r) = Er^k - \beta_1 n_1(r) \tag{21}$$

The constant E can be found imposing the boundary condition (2.7), which truncated at the first order, leads to

$$p_1(R^*) = \sigma\frac{k^2-1}{R^{*2}} - \frac{\partial p^*}{\partial r}(R^*) = \sigma\frac{k^2-1}{R^{*2}} + \beta n_0 \frac{I_1(R^*)}{I_0(R^*)}\,. \tag{22}$$

The value of the coefficient E, valid for $\lambda \neq -1$ is reported in Table 1. Finally, the dispersion equation can be derived from the condition (2.9), considering only the first order terms

$$\lambda = -p^{*\prime\prime}(R^*) - p_1'(R^*)\,. \tag{23}$$

The expression for the dispersion equation as a function of the dimensionless parameters β, σ, R^* and R_{out} is reported in Table 1, for $\lambda \neq -1$. These dispersion relations relate the growth mode λ to the wave-number k in an implicit way and should be solved through numerical iteration technique.

The dispersion equation includes also the case $\lambda = 0$, with the notation $A_\lambda = A$ when $\lambda \neq \{0, -1\}$ and $A_\lambda = A_0$ when $\lambda = 0$. The value of the coefficient A_0 is defined as $A_0 = \lim_{\lambda\to 0} A_\lambda$, which leads to

$$A_0 = n_0\left(R^{*2k} - R_{out}^{2k}\right) / \left[2kR^{*2k-1}I_k(R^*) - \left(R^{*2k} - R_{out}^{2k}\right)I_{k-1}(R^*)\right]\,.$$

References

[1] Friedl P., Hegerfeldt Y., Tusch M., "Collective cell migration in morphogenesis and cancer." *Int. J. Dev. Biol.* 48, 441-449 2004

[2] Poujade M., Grasland-Mongrain E., Hertzog A., Jouanneau J., Chavrier P., Ladoux B., Buguin A., Silberzan P. 2007 "Collective migration of an epithelial monolayer in response to a model wound." *PNAS* 104, 15988-15993.

[3] Dockery J., Klapper I. 2001 "Finger formation in biofilm layers." *SIAM J. Appl. Math.* 62, 853869.

[4] Byrne H.M. 1999 "A weakly nonlinear analysis of a model of avascular tumor growth." *J. Math. Biol.* 39, 59-89.

[5] Ben Amar M., Chatelain C., Ciarletta P. 2011 "Contour Instabilities in Early Tumor Growth Models." *Phys. Rev. Lett.* 106, 148101.

[6] Greenspan H.P. 1976 "On the growth and stability of cell cultures and solid tumors." *J. Theor. Biol.* 56, 229-243.

[7] Weijer C.J. 2009 "Collective cell migration in development." *J. Cell Sci.* 122, 3215-3223.

[8] Martin P., Parkhurst S.M. 2004 "Parallels between tissue repair and embryo morphogenesis." *Development* 131, 3021-3034.

[9] Murray J.D., Oster G.F., Harris A.K. 1983 "Mechanical aspects of mesenchymal morphogenesis." *J. Embryol. Exp. Morph.* 78, 83-125.

[10] Zhang H.P., Beer A., Florin E.L., Swinney H.L. 2010 "Collective motion and density fluctuations in bacterial colonies." *PNAS* 107, 13626-13630.

[11] Ben-Jacob E., Schultz D. 2010 "Bacteria determine fate by playing dice with controlled odds." *PNAS* 107, 13197-13198.

[12] Friedl P. and Gilmour D. 2009 "Collective cell migration in morphogenesis, regeneration and cancer." *Nat. Rev. Mol. Cell Biol.* 10, 445-457.

[13] Be'er A., Zhang H. P., Florin E.L., Payne S.M., Ben-Jacob E., Swinney H.L. 2009 "Deadly competition between sibling bacterial colonies." *PNAS* 106, 428-433.

[14] Manz B.N., Groves J.T. 2010 "Spatial organization and signal transduction at intercellular junctions." *Nat. Rev. Mol. Cell Biol.* 11, 342-352.

[15] DuFort C.C., Paszek M.J., Weaver V.M. 2011 "Balancing forces: architectural control of mechanotransduction." *Nature Rev. Mol. Cell Biol.* 12, 308-319.

[16] Stylianopoulos T., Martin J.D., Chauhan V.P., Jain S.R., Diop-Frimpong B., Bardeesy N., Smith B.L., Ferrone C.R., Hornicek F.J., Boucher Y. et al. 2012 "Causes, consequences, and remedies for growth-induced solid stress in murine and human tumors." *PNAS* 109, 15101-15108.

[17] Ingber D.E. 2006 "Cellular mechanotransduction: putting all the pieces together again." *FASEB J.* 20, 811-827.

[18] Ben-Jacob E., Cohen I., Gutnick D. L. 1998 "Cooperative organization of bacterial colonies: from genotype to morphotype." *Annu. Rev. Microbiol.* 52, 779-806.

[19] Ben-Jacob E., Cohen I., Levine H. 2000 "Cooperative self-organization of microorganisms." *Adv. Phys.* 49, 395-554.

[20] Fujikawa H., Matsushita M. 1989 "Fractal Growth of Bacillus subtilis on Agar Plates." *J. Phys. Soc. JPN.* 58, 3875-3878.

[21] Fujikawa H. 1994 "Diversity of the growth patterns of Bacillus Subtilis colonies on agar plates." *FEMS Microbiol. Ecol.* 13, 159168.

[22] Kawasaki K., Mochizuki A., Matsushita M., Umeda T., Shigesada N. 1997 "Modeling spatio-temporal patterns generated by Bacillus Subtilis." *J. Theor. Biol.* 188, 177-185.

[23] Matsushita M., Hiramatsu F., Kobayashi N., Ozawa T., Yamazaki Y., Matsuyama Y. 2004 "Colony formation in bacteria: experiments and modeling." *Biofilms* 1, 305-317.

[24] Be'er A., Strain S. K., Hernández R. A., Ben-Jacob E. and Florin E.L. 2013 "Periodic Reversals in Paenibacillus dendritiformis Swarming." *J Bacteriol.* 195(12): 2709-2717.

[25] Wu Y., Kaiser A. D., Jiang Y. and Alber M.S. 2009 "Periodic reversal of direction allows Myxobacteria to swarm." *PNAS* 106(4), 1222-1227.

[26] Ben-Jacob E., Levine H. 2006 "Self-engineering capabilities of bacteria." *J. R. Soc. Interface* 3, 197-214.

[27] Farrell F.D.C., Hallatschek O., Marenduzzo D., Waclaw B. 2013 "Mechanically driven growth of quasi-two dimensional microbial colonies." *Phys. Rev. Lett.* 111, 168101.

[28] Bonachela J.A., Nadell C.D., Xavier J. B., Levin S.A. 2011 "Universality in bacterial colonies." *J. Stat. Phys.* 144, 303-315.

[29] Picioreanu C., van Loosdrecht M.C., Heijnen J.J. 1998 "A new combined differential-discrete cellular automaton approach for biofilm modeling: application for growth in gel beads." *Biotechnol. Bioeng.* 57, 718-731.

[30] Matsushita M., Wakita J., Itoh H., Ràfols I., Matsuyama T., Sakaguchi H., Mimura M. 1998 “Interface growth and pattern formation in bacterial colonies.” *Phys. A* 249, 517-524.

[31] Kozlovsky Y., Cohen I., Golding I., Eshel Ben-Jacob E. 1999 Lubricating Bacteria Model for Branching growth of Bacterial Colonies. *Phys. Rev. E Stat. Phys. Plasmas Fluids Relat. Interdiscip. Topics.* **59**(6), 7025-35.

[32] Mimura M., Sakaguchi H., Matsushita M. 2000 “Reaction-diffusion modelling of bacterial colony patterns.” *Phys. A* 282, 283-303.

[33] Marrocco A., Henry H., Holland I.B., Plapp M., Sé ror S. J., Perthame B. 2010 “Models of self-organizing bacterial communities and comparisons with experimental observations.” *Math. Model. Nat. Phenom.* 5, 148-162.

[34] Wakita J., Komatsu K., Nakahara A., Matsuyama T., Matsushita M. 1994 “Experimental investigation on the validity of population dynamics approach to bacterial colony formation.” *J. Phys. Soc. JPN.* 63, 1205-1211.

[35] Golding I., Kozlovsky Y., Cohen I., Ben-Jacob E. 1998 “Studies of bacterial branching growth using reaction-diffusion models for colonial development.” *Phys. A* 260, 510-554.

[36] Korolev K.S., Müller M.J.I., Karahan N., Murray A.W., Hallatschek O., Nelson D.R. 2012 “Selective sweeps in growing microbial colonies.” *Phys. Biol.* 9, 026008.

[37] Keller E.F., Segel L.A. 1971 “Model for chemotaxis.” *J. Theor. Biol.* 30, 225-234.

[38] Graziano L., Preziosi L. 2007 “Mechanics in tumor growth. In *Modeling of Biological Materials”*, F. Mollica, K. R. Rajagopal, L. Preziosi, Eds., p. 267-328, Birkhäuser Boston.

[39] Lega J., and Passot T. 2003 “Hydrodynamics of bacterial colonies: A model.” Phys. Rev. E 67, 031906

[40] Verdier C., Etienne J., Duperray A., Preziosi L. 2009 “Review. Rheological properties of biological materials.” *Comptes Rendus de l’Académie des Sciences* - Series IV - Physics, 10, 790-811.

[41] Adler J. 1966 “Chemotaxis in bacteria.” *Science* 153, 708-716.

[42] Flemming H.C., Wingender J. 2010 “The biofilm matrix.” *Nature Rev.* 8, 623-633.

[43] Cross M.C., Hohenberg P.C. 1993 “Pattern formation outside of equilibrium.” *Rev. Mod. Phys.* **65**.

[44] Homsy G. M. 1987 “Viscous fingering in porous media.” *Ann. Rev. Fluid Mech.* **19**, 271-311.

[45] Paterson L. 1981 “Radial fingering in a Hele Shaw cell.” *J. Fluid. Mech.* **113**, 513-529.

[46] Langer J.S. 1980 “Instabilities and pattern formation in crystal growth.” *Rev. Mod. Phys.* **52**, 1-30.

[47] Saffman P. G. and Taylor G. 1958 “The penetration of a fluid into a medium or hele-shaw cell containing a more viscous liquid.” *Proc. Soc. London, Ser A* 245: 312-329.

[48] http://www.freefem.org

[49] Wakita J., Itoh H., Matsuyama T., Matsushita M. 1997 “Self-Affinity for the Growing Interface of Bacterial Colonies.” *J. Phys. Soc. JPN.* 66, 67-72.

[50] Ford R.M., Lauffenburger D.A. 1991 “Analysis of chemotactic bacterial distributions in population migration assays using a mathematical model applicable to steep or shallow attractant gradients.” *Bull. Math. Bio.* 53, 721-749.

[51] Zhou S., Lo W.C., Suhalim J.L., Digman M.A., Gratton E., Nie Q., Lander A.D. 2012 “Free extracellular diffusion creates the Dpp morphogen gradient of the Drosophila wing disc.” *Curr. Biol.* 22, 668-675.

[52] Yu S.R., Burkhardt M., Nowak M., Ries J., Petrášek Z., Scholpp S., Schwille P., Brand M. 2009 “Fgf8 morphogen gradient forms by a source-sink mechanism with freely diffusing molecules.” *Nature* 461, 533-537.

[53] Ben Amar M. 2013 “Chemotaxis migration and morphogenesis of living colonies.” *Eur. Phys. J. E.* 36, 64.

[54] Ziebert F., Aranson I.S. 2013 “Effects of adhesion dynamics and substrate compliance on the shape and motility of crawling cells.” *PLoS One* 8, e64511.

[55] Tindall M.J., Maini P.K., Porter S.L., Armitage J.P. 2008 “Overview of Mathematical Approaches Used to Model Bacterial Chemotaxis II: Bacterial Populations.” *Bull. Math. Bio.* 70, 1570-1607.

[56] Eberl H.J., Parker D.F., van Loosdrecht M.C.M. 2001 “A new deterministic spatio-temporal continuum model for biofilm development.” *J. Theor. Med.* 3, 161-175.

[57] Roca-Cusachs P., Sunyer R., Trepat X. 2013 “Mechanical guidance of cell migration: lessons from chemotaxis.” *Curr. Opin. Cell Biol*. 25, 543-549.

[58] Cochet-Escartin O., Ranft J., Silberzan P., Marcq P. 2014 “Border Forces and Friction Control Epithelial Closure Dynamics.” *Biophys. J.* 106, 65-73.

MOX Technical Reports, last issues

Dipartimento di Matematica "F. Brioschi",
Politecnico di Milano, Via Bonardi 9 - 20133 Milano (Italy)

57/2014 Giverso, C.; Verani, M.; Ciarletta P.;
Branching instability in expanding bacterial colonies

55/2014 Antonietti, P. F.; Houston P.; Sarti, M.; Verani, M.
Multigrid algorithms for hp-version Interior Penalty Discontinuous Galerkin methods on polygonal and polyhedral meshes

56/2014 Antonietti, P. F.; Sarti, M.; Verani, M.; Zikatanov, L. T.
A uniform additive Schwarz preconditioner for the hp-version of Discontinuous Galerkin approximations of elliptic problems

54/2014 Ferrario, E.; Pini, A.
Uncertainties in renewable energy generation systems: functional data analysis, monte carlo simulation, and fuzzy interval analysis

53/2014 Ieva, F.; Paganoni, A.M., Pietrabissa, T.
Dynamic clustering of hazard functions: an application to disease progression in chronic heart failure

52/2014 Dede , L..; Quarteroni, A.; S. Zhu, S.
Isogeometric analysis and proper orthogonal decomposition for parabolic problems

51/2014 Dassi, F.; Perotto, S.; Formaggia, L.
A priori anisotropic mesh adaptation on implicitly defined surfaces

50/2014 Bartezzaghi, A.; Cremonesi, M.; Parolini, N.; Perego, U.
An explicit dynamics GPU structural solver for thin shell finite elements

49/2014 D. Bonomi, C. Vergara, E. Faggiano, M. Stevanella, C. Conti, A. Redaelli, G. Puppini et al
Influence of the aortic valve leaflets on the fluid-dynamics in aorta in presence of a normally functioning bicuspid valve

48/2014 Penta, R; Ambrosi, D; Shipley, R.
Effective governing equations for poroelastic growing media